IMPRESSION CREEP STUDIES ON SIMULATED REHEATED HAZ OF P91 AND P91B STEELS

Akhil Khajuria[1], Rajneesh Kumar[2], Raman Bedi[3], Jaganathan Swaminanthan[4], Dinesh Kumar Shukla[5]

[1,3,5]National Institute of Technology Jalandhar, Department of Mechanical Engineering
Punjab, India, 144011
[2,4]CSIR – National Metallurgical Laboratory
Jamshedpur, India, 831007

Corresponding author: Raman Bedi, E-mail address: bediraman74@gmail.com

Abstract: Effect of boron modified microstructure on creep behaviour of simulated HAZ produced on reheating passes has been examined by impression creep technique. Short duration creep tests for 20 hours were run at 625°C and 365 MPa on simulated P91 and P91B multipass HAZs representing CG + FGHAZ and CG + ICHAZ as well as on as received steel alloys of P91 and P91B. It is revealed that presence of 100ppm boron in P91 steel enhances the lath martensite structure which reduces variation in creep deformation behaviour among P91B base metal and P91B multi-pass weld HAZs. Whereas absence of boron in P91 leads to coarsening of precipitates on subsequent weld thermal cycles which leads to an increase in variation of creep deformation behaviour among P91 base metal and P91 multi-pass HAZs. This makes P91 - HAZ as a weakest link in boron free P91 weldments and therefore prone to type IV cracking.

Keywords: P91 steel, effect of boron, Gleeble™ simulation, reheated HAZ, microstructure, impression creep.

1. INTRODUCTION

The demand to enhance efficiency and reduction in CO_2 emissions has given thrust to increase operating temperatures and pressures of power generating units. P91, ferritic/martensitic steel, is one such special low carbon alloy which has been empowering power plant industry from four decades particularly due to its better creep strength than austenitic steels (Klueh, 2009). Manufacturing components of P91 steel like boiler headers, super heater tubes etc. in thermal power plants require fusion welding, since they are generally thick sections and it is difficult to join them by low heat input welding processes such as tungsten inert gas welding or electron beam welding (Goswami, 2010). Therefore high heat input welding processes like submerged arc welding are employed for producing P91 weldments. But, thermal cycles of fusion welding lead to undesirable microstructural changes due to phase transformations at heat affected zone (HAZ) of weldment degrading mechanical as well as creep properties with respect to virgin state of P91 steel (Wang et al., 2016). Such deprivation in creep strength leads to premature in-service failure of P91 weldments at outer HAZ by Type IV cracking (Wang and Li, 2016). Type IV cracking is intergranular cracking which occurs due to microstructural heterogeneity among sub-zones of HAZ. To overcome this issue, addition of 100ppm boron in virgin P91 steel has been found useful for enhancing creep life of P91 welded joints, but still final creep rupture takes place due to type IV cracking (Baral et al., 2015). To maintain smooth functioning of power plants, repairing pre-existing P91 joints suits as a better option instead of substituting them with new joints due to economic reasons. But, repairing a fusion welded joint add up thermal cycles to the existing P91- HAZ whose microstructure is again affected due to multi-layer fusion welding (Łomozik and Tasak, 2006). For multi-phase steels like P91 (P91 contains $M_{23}C_6$, MX particles), formation of a subzone in HAZ is governed by phase transformation temperatures Ac_1 and Ac_3, since secondary phase particles affect martensite to austenite transformation and subsequently by maximum peak temperature reached in a particular subzone of HAZ (Porter et al., 2009). $M_{23}C_6$ carbides (M = Cr, Fe, Mo) have FCC type of crystal structure and they help to stabilise martensite laths whereas, MX (M = Nb, V, Ti and X = C, N) particles retard both grain growth and creep deformation by pinning on grain boundaries. Therefore for single pass weld thermal cycle case, based on decline in peak temperature from weld metal towards base metal, HAZ is formed into three distinguishable subzones usually named after grain size and phase transformation temperature i.e. coarse grain HAZ (CGHAZ), fine grain HAZ (FGHAZ) and inter-critical HAZ (ICHAZ) as shown in Figure 1.

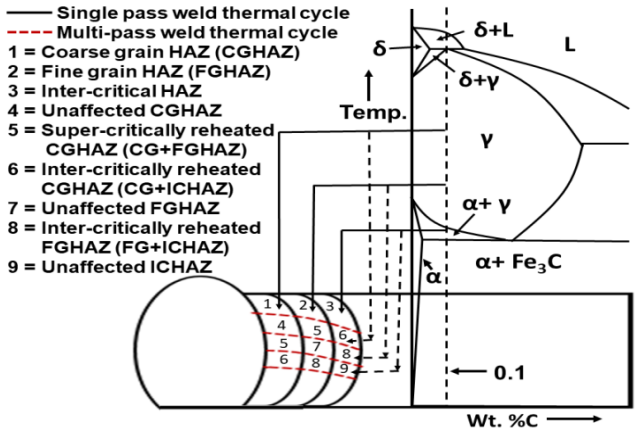

Fig. 1. Schematic representing evolution of subzones of HAZ after multiple passes of weld thermal cycles

However, development of microstructure at HAZ due to multiple weld thermal cycles is significantly different, since overlaying successive layers of weld bead produce successive thermal cycles affecting previous existing subzone of HAZ (Wang et al., 2017). The successive layers of subzones of HAZ evolve after triggering reheating of previous CGHAZ during welding multi-pass thermal cycles. Hence, HAZ subzones formed after multi-pass welding are named according to the degree of heating. For example, if previous CGHAZ is reheated to a peak temperature of FGHAZ, sub-HAZ formed due to this heating is referred as CG + FGHAZ or super-critically reheated CGHAZ. Similarly, if degree of heating on CGHAZ corresponds to a peak temperature of ICHAZ, then sub-HAZ formed is referred as CG + ICHAZ or inter-critically reheated CGHAZ and so on. To address mechanical behaviour of engineering materials, micro indendation techniques have proven to be worthy (Ciofu and Creţu, 2014). Impression creep is a pioneering development among creep testing methods for characterizing creep behaviour of creep resistant materials as it uses specimens of small dimensions and less test time than conventional methods of creep testing (Yang and Li, 2013). This technique becomes more useful when volume of material to be evaluated for knowing creep properties is inherently small like HAZ in weldments whose size falls in the range of 2 – 3 mm even for high heat inputs of fusion welding (Vijayanand et al., 2014). With the availability of thermo mechanical simulator like Gleeble™, exact replicas of thermally treated microstructures in subzones of HAZ could be produced (Akhtar, 2017). Such simulated samples can be further used for studying creep behaviour by impression creep technique. Creep resistance of a P91 - HAZ subzone is dependent on its microstructure evolved after receiving a particular weld thermal cycle which significantly alters fraction of micro-constituents of designed virgin alloy. Numerous studies have been reported on creep behaviour of subzones of P91-HAZ representing single pass weld thermal cycle. However, creep behaviour of HAZ subzones of boron free and boron added P91 originating from multi-pass weld thermal cycles has not so far been reported. The objective of current paper is to examine impression creep behaviour of subzones of Gleeble™ simulated reheated HAZ of P91 and P91B steels.

2. EXPERIMENTAL PROCEDURE

2.1 Steels

As received heats of P91 and P91B were subjected to two furnace heat treatments comprising of normalizing at 1050 ^{o}C/30 min and then tempering at 760^{o}C/2h. Chemical composition of P91 and P91B are shown in Table 1.

Table 1. Chemical composition of P91 and P91B in wt.%

Element	C	Cr	Mo	V	Nb	N	B	Fe
	%							
P91	0.11	9.44	0.71	0.2	0.05	0.06	-	Bal.
P91B	0.10	8.26	0.88	0.186	0.06	0.004	0.01	Bal.

2.2 Gleeble™ simulation of multi-pass HAZ

The prerequisites for multi-pass HAZ simulation are heat input (KJ/mm), heating rate – HR (^{o}C/s), peak temperature -T_p (^{o}C), hold time at T_p (s), inter-pass temperature, and cooling rate (^{o}C/s) or $t_{8/5}$ (s). Heat input, heating rate, cooling rate and inter-pass temperature were found from thermal data acquisition (DAQ) system employed during submerged arc welding (SAW) of 11 mm thick plates of P91. SAW for joining of 11 mm butt joint of P91 corresponded to a heat input of 2.5 KJ/mm. After analysis of DAQ data, $t_{8/5}$ = 30 seconds was selected which represents a cooling rate of 10 °C/s during exponential cooling from 800 ^{o}C to 500 ^{o}C with linear heating at heating rate of 100 °C/s. In case of transformable steels, peak temperatures for subzones of HAZ simulations are kept according to phase transformation temperatures i.e. Ac_1 and Ac_3. For determining Ac_1 and Ac_3, dilatometric experiments on standard dumb bell shaped specimens as per ASTM-1033 were carried out on P91 and P91B steels on continuous cooling transformation unit of thermo-mechanical simulator-Gleeble™ 3800. Thereafter, peak temperatures for multipass HAZ simulations of P91 and P91B were decided to carry out thermal simulations on Gleeble™. All thermal simulations were conducted on square HAZ simulation samples with dimensions 78 mm × 11 mm × 11 mm with copper grips and a span of 30 mm as shown in Figure 2.

Two thermocouples of K type were spot welded for monitoring programmed temperature and obtaining real time simulation temperature data with respect to time. The exponential cooling from peak temperature was programmed as per equation (1).

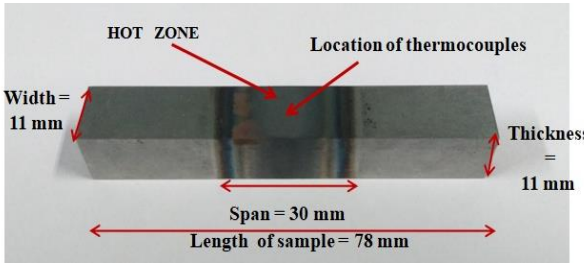

Fig. 2. Gleeble™ simulated P91 - HAZ sample

$$T = T_P \times e^{-0.47t/\Delta t} \quad (1)$$

where T = instantaneous temperature (°C), t = time (s) and Δt = time to cool from 800 °C to 500°C (s). Summary of dilatometric experiments on Gleeble™ is presented in Table 2. Thermal profile data of simulated HAZ as obtained from QuickSIM inbuilt software with Gleeble™ was plotted on Originlab plotting tool. Plots of thermal profiles between peak temperatures versus time are shown in Figure 3.

Table 2. CCT data for multi-pass HAZ simulations of P91 and P91B steels

CCT	HR [°C/s]	T_p [°C]	Hold at T_p [s]	CR [°C/s]	Ac1 and Ac3 [°C]
P91	100	1100	20	10	885 and 965
P91B	100	1100	20	10	933 and 1040

It can be noted from simulated thermal profiles of P91B in Figure 3(b) that higher peak temperatures have been taken for simulation of second cycle of FGHAZ and ICHAZ, since transformation temperatures Ac_1 and Ac_3 of P91B steel are higher than P91 as revealed by dilatometry experiments. Whereas simulation of first cycle of CGHAZ was carried out at same peak temperature (1240 °C) for both steels because maximum temperature measured by DAQ in this subzone of HAZ is exceedingly larger than Ac_3 of P91 and P91B.

2.3 Specimen preparation for microstructural characterization and impression creep tests

Simulated specimens were cut from thermocouple spot weld location by wire EDM exposing two surfaces for microstructural investigation and creep tests. After taking out hot region from simulated specimens, a post weld heat treatment (PWHT) for 760 °C/3h was given in a muffle furnace.

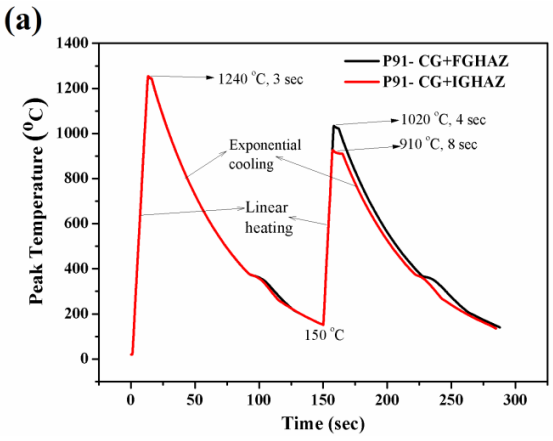

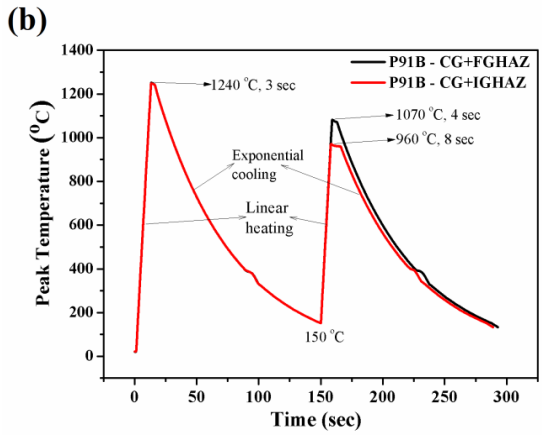

Fig. 3. Thermal profiles of simulated multi-pass HAZs of P91 and P91B steels

The exposed surfaces of thermocouple spot weld location were prepared for optical and scanning electron microscopy. Mechanical polishing of these surfaces by using emery papers was done for removing deep scratches. This was followed by cloth polishing with the use of alumina and water for removing the fine scratches from the sample surface to achieve mirror like appearance. These prepared surfaces were etched with 28% Nital (HNO_3 + C_2H_5OH). Same method was followed for sample preparation of as received steels. Heyn's linear intercept method was used to measure prior austenite grain (PAG) size. For impression creep tests, samples of dimensions 10mm × 10mm × 10mm were used. Creep tests were performed on Spranktronics impression creep testing machine (Figure 4) at 625 °C and a punching stress of 365MPa corresponding to uniaxial creep stress of 110MPa in order to satisfy a correlation factor of 3.3 as specified in literature (Yu and Li, 1977). An indenter of nimonic alloy with 2 mm diameter was used for this purpose.

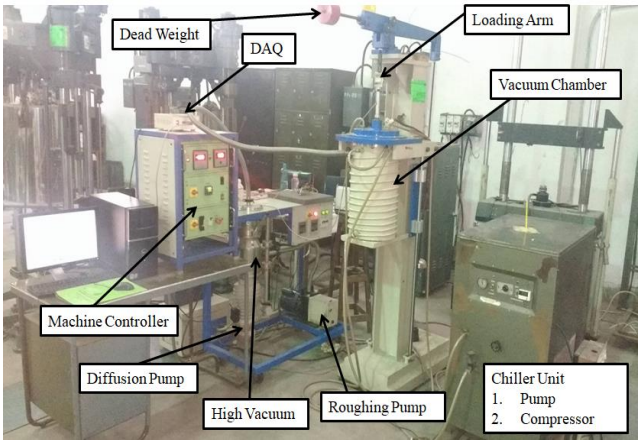

Fig. 4. Set up for impression creep tests

3. RESULTS AND DISCUSSIONS

3.1 Microstructures of base metals

Both microstructures of P91 and P91B steels as observed in Figures 5(a)-(b) show tempered martensitic structures with only difference in PAG size. P91 has a

smaller PAG size of 18 µm than 28 µm in P91B. Existence of a bigger PAG size is attributed to the effect of boron which decreases the grain boundary energy and allows grain growth in P91B. Also, prior austenite grain boundaries (PAGBs) in P91B appear to avoid cellular grain structure in P91B. Martensitic laths show healthy presence and are oriented in identical directions inside PAGBs of P91B in contrast to P91 where owing to small PAGs, relatively weak lath martensitic structure is observed. SEM micrograhs in Figures 5(b)-(d) represent distinguishing features among both heats. Coarse precipitates with large inter particle distance are apparent on PAGBs of P91whereas a fine distribution of precipitates exist in P91B steel. Regions marked in red colored broken line box and circle indicates transfomed and untranformed regions respectively in P91B. The untransfomed region appears to be large in P91B than P91 which is the effect of boron on delaying phase transformation i.e. austenization during normalizing and therefore stabilization of ferrite.

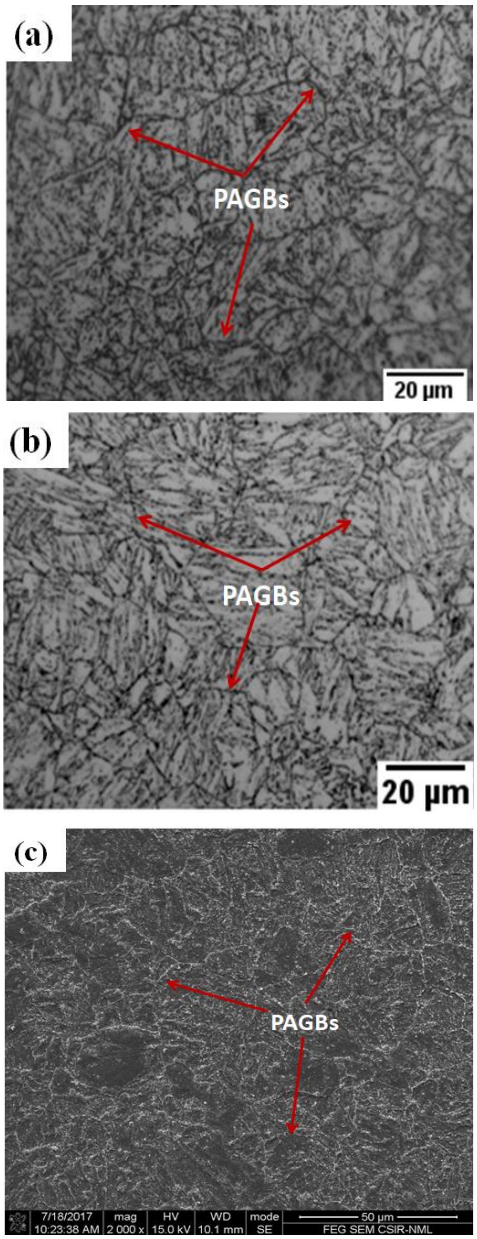

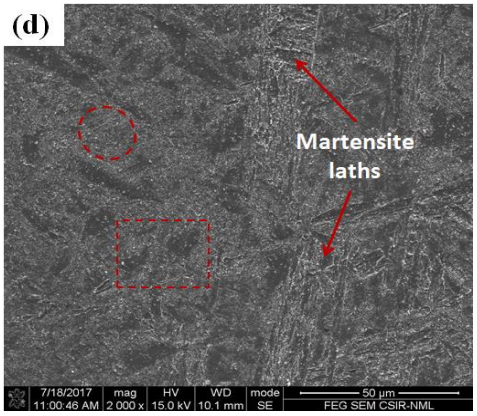

Fig. 5. Photomicrographs of base metals
(a) (c) P91 (b) (d) P91B

3.2 Microstructures of simulated P91 and P91B HAZs

3.2.1 Supercritically reheated CGHAZ

Figures 6(a) and (b) show photomicrographs of supercritically reheated CGHAZ of P91 and P91B steels. It can be observed in Figure 6(a), that a microstructure comprising of big grains with neighbouring small grains is obtained in P91 - CG + FGHAZ with an average PAG size of 31 µm. The first thermal cycle during this simulation went to a peak temperature of 1240 ºC which corresponds to CGHAZ resulting in coarsening of grains and subsequently second thermal cycle of FGHAZ slightly influences the microstructure leading to formation of small grains. FGHAZ thermal cycle induces heterogeneity and leaves excessive secondary precipitation across the microstructure. Martensite laths as noticed inside of marked PAGs are randomly oriented.

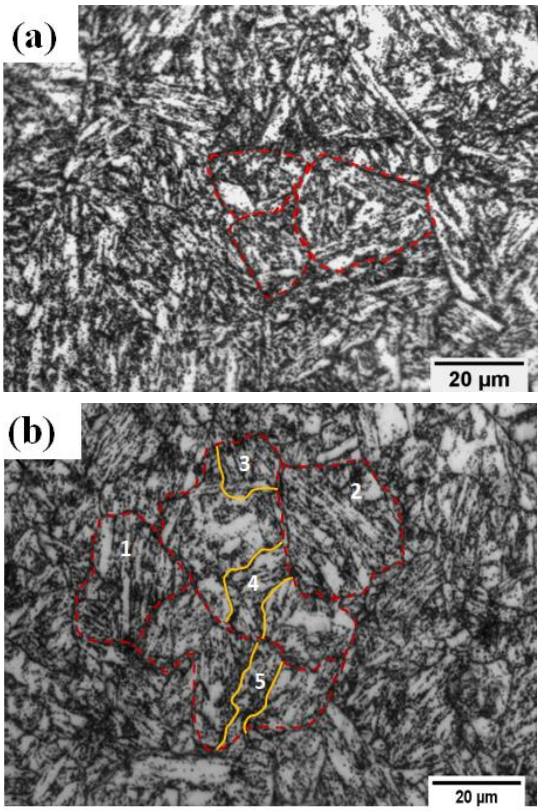

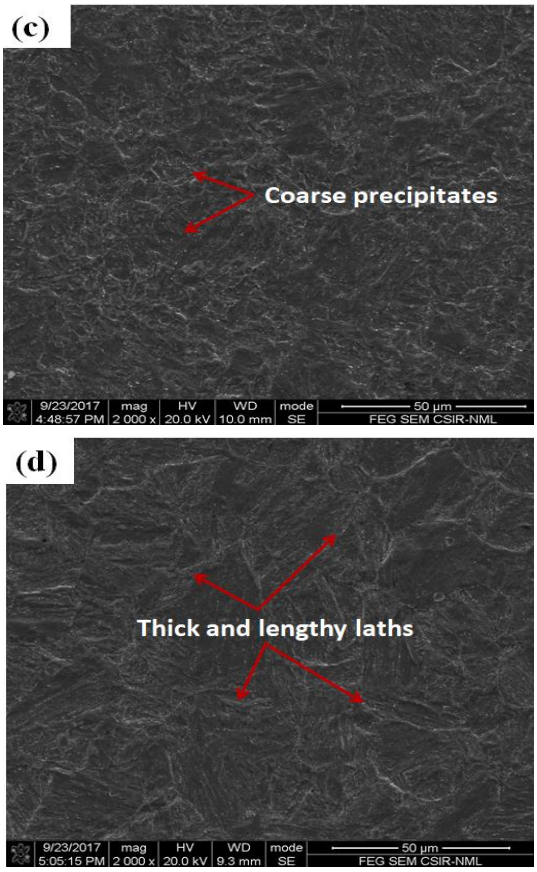

Fig. 6. Photomicrographs of CG + FGHAZ after PWHT (a) (c) P91 (b) (d) P91B

Similar observations are noted for P91B – CG + FGHAZ too other than PAG size which is of the same order of 28 µm as in as received state of P91B steel.

In addition to PAG size, differences are prominent for preferred lath orientation which is evident in marked PAG 1 and 2. Evolution of small PAGs marked as 3, 4, 5 with neighbouring PAGs of CGHAZ thermal cycle is dominant in P91B – CG + FGHAZ. This is attributed to low dissolution temperature of boron containing precipitates. Low magnification SEM micrographs of P91 - CG + FGHAZ and P91B - CG + FGHAZ in Figures 6(c)-(d) respectively discern detailed microstructural differences among both simulations. It is unambiguous that second thermal cycle of FGHAZ leads to coarsening of precipitates on PAGBs in P91. On the contrary, thick and lengthy laths evolve with negligible precipitate coarsening in P91B after second thermal cycle of FGHAZ. Fine precipitates are decorated on lath boundaries in P91B – CG + FGHAZ which signifies stabilization of lath martensite structure on addition of 100ppm boron in P91 steel.

3.2.2 Intercritically reheated CGHAZ

Figure 7(a) show photomicrograph of intercritically reheated P91 - CGHAZ which depicts that partial transformation of martensite is prevalent. Since peak temperature during second thermal cycle in this simulation corresponds to ICHAZ, martensite doesn't get sufficient energy to fully transform to austenite and therefore final microstructure after PWHT cycle is only tempered with the presence of mixed grains of partially transformed martensite and tempered martensite. However, this is not the case in P91B – CG + ICHAZ. A fully martensitic microstructure with a PAG size of 28 µm is observed. This is attributed to the presence of boron which stabilizes the microstructure even after weld thermal cycle and PWHT. Formation of small PAGs is evident in Figure 7(b).

Coarsening of precipitates is clearly seen in SEM micrograph of P91 – CG + ICHAZ (Fig. 7c) whereas needle shaped martensite with uniform distribution of precipitates is observed in P91B – CG + ICHAZ (Figure 7d).

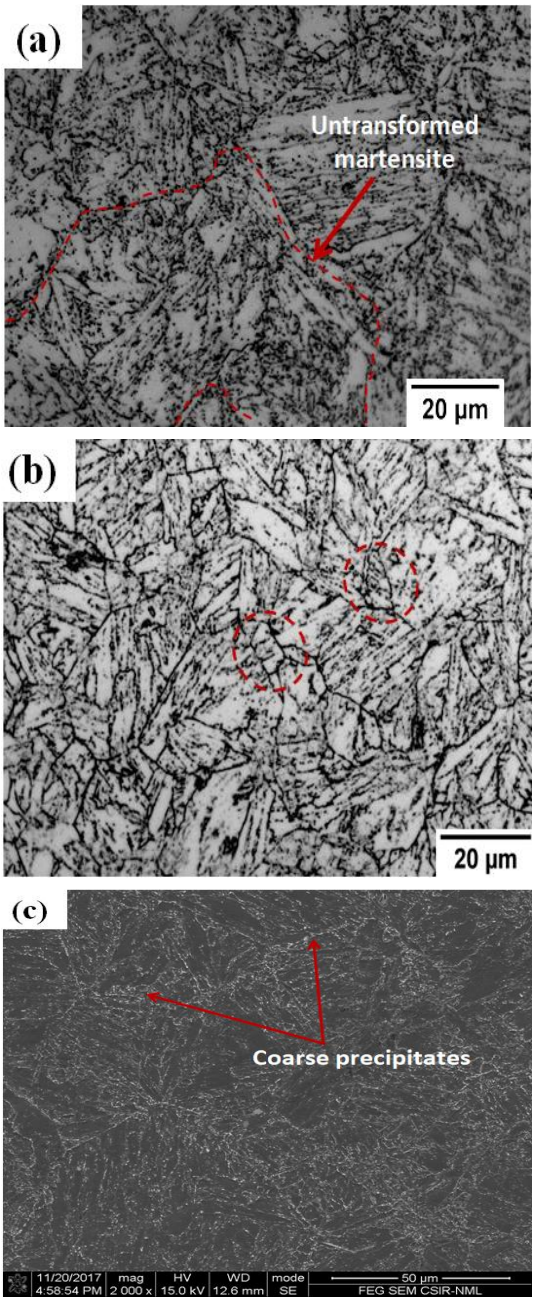

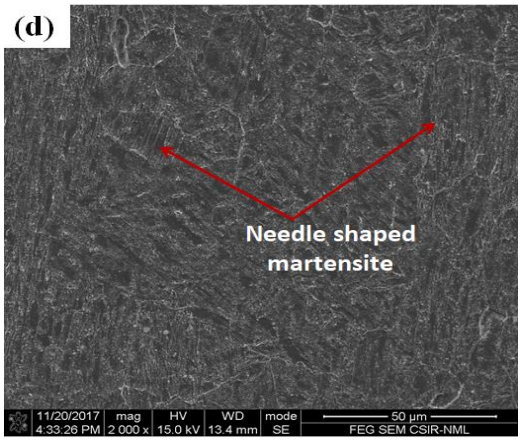

Fig. 7. Photomicrographs of CG + ICHAZ after PWHT (a) (c) P91 (b) (d) P91B

3.3 Impression creep behaviour of base metals and simulated HAZs

During an impression creep test; the loaded sample is deformed locally which produces a deformed plastic zone underneath an indentor as shown in Figures 8(a)-(b). The rate of creep deformation produced in a sample is dependent on the microstructure of material subjected to compression loading, temperature during impression creep test and diameter of indentor. The impression creep curves between depth of penetration (DOP) and time for 20 hours of creep exposure at 365 MPa and 625ºC presenting comparison of creep behaviour among base metals and their simulated multi-pass HAZs are shown in Figure 9.

It is obvious from Figure 9(a) that base metal of P91 show least resistance to punching stress and reaches to maximum DOP within the same duration of creep test which can be held responsible to least PAG size and coarse precipitates in P91 steel.

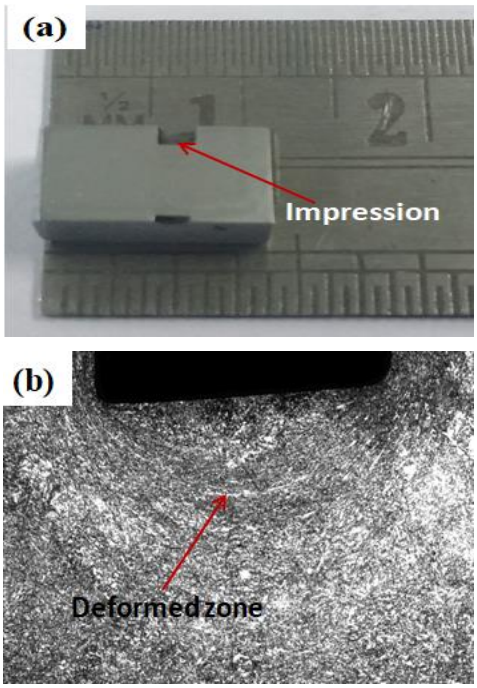

Fig. 8. Impression creep of base metal P91B (a) Crept sample after creep test (b) Evolution of deformed plastic zone underneath the indentor

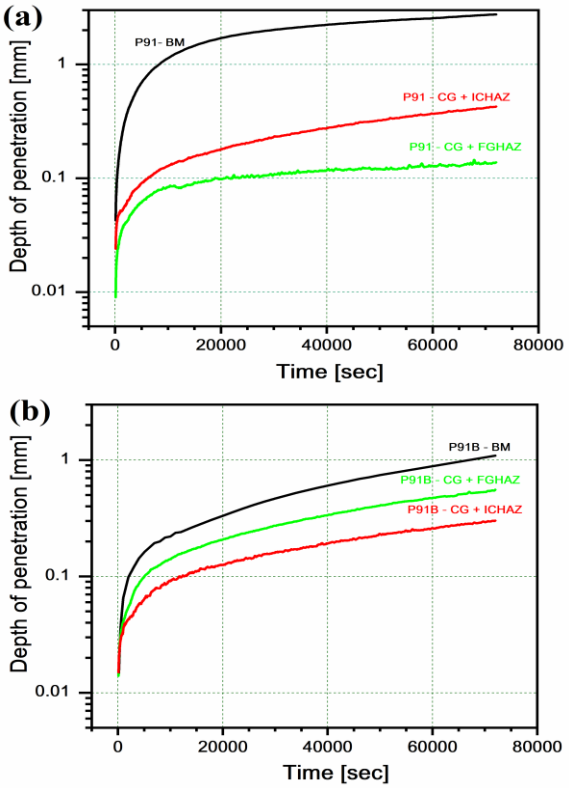

Fig. 9. Impression creep curves at 365 MPa and 625ºC. (a) P91 and reheated HAZs of P91 (b) P91B and reheated HAZs of P91B

Presense of coarse particles on PAGBs decrease grain boundary pinning during elevated temperatures and allow easy grain sliding which degrades creep resistance. P91 – CG + FGHAZ happens to most creep resistant in P91 group which produces a large gap in maximum DOP achieved among it and base metal of P91 thus increasing variation in creep behaviour. On the other hand, relatively bigger PAG size of P91B with fine precipitates on PAGBs than P91 show mild improvement in creep resistance as observed in Figure 9(b). Maximum DOP reached in same duration of impression creep falls in a close range for simulated reheated HAZs of P91B and base metal of P91B indicating accomplishment of nearly homogenous creep behaviour which is attributed to role of boron in microstructural stabilization after HAZ simulation and PWHT. It is pertinent to mention here that an increased fraction of small PAGs in supercritically reheated CGHAZ of P91B slightly decreases creep resistance than its counterpart. However, such phenomenon adds up as an advantage in maintaining uniform creep behaviour in boron modified P91 weldments. Creep rate plots as obtained from impression creep testing machine for both P91, P91B base metals and their simulated HAZs after PWHT are shown in Figure 10. It is evident that both base metals deform at a maximum creep rate than sub –HAZs. Nevertheless, uniformity in creep deformation rate is achieved in presence of boron in P91 steel which ultimately delays type IV cracking in its weldments.

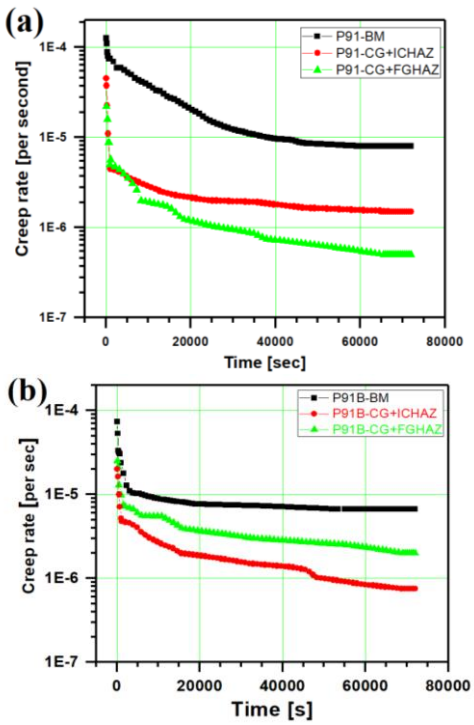

Fig. 10. Creep rate curves at 365 MPa and 625 ºC (a) P91 and reheated HAZs of P91 (b) P91B and reheated HAZs of P91B

4. CONCLUSIONS

No effect on an average PAG size is observed in simulated reheated CGHAZ of P91B steel i.e. supercrictically reheated CGHAZ and intercrtically reheated CGHAZ with respect to virgin P91B steel inferring stabilization of HAZ microstructure after multi –pass welding and subsequent PWHT.

Coarse precipitates on PAGBs in P91 steel leads to easy grain boundary sliding during impression creep and therefore increased creep rate. On the contrary, fine precipitates with uniform distribution across the microstructure retards creep rate in base metal P91B and its HAZs.

Presence of boron in P91 not only enhances creep resistance of this steel, but also produces nearly homogenous creep behaviour among base metal of P91B and subzones of P91B – HAZ.

Existence of mixed grains of partially transformed martensite and tempered martensite weakens the microstructure and therefore poor creep resistance is shown by P91 – intercrtically reheated CGHAZ as in contrast to P91B – intercrtically reheated CGHAZ where fully tempered martensitic structure is observed which comparatively better creep resistance to same punching stress of 365 MPa at 625 ºC.

The impression creep technique is found sensitive to base metals of boron free and boron added P91 steel as well as different simulated multi-pass HAZ specimens of P91 and P91B. This infers that effect of heat treatments on creep resistant steels and their weld HAZs could be quickly characterized for creep behaviour using short duration impression creep tests.

REFERENCES

1. Klueh, R.L., (2009). *Ferritic/martensitic steels for advanced nuclear reactors*, Trans. Indian Inst. Met., 62(2), 81-87.

2. Goswami, P., (2010). *P (T) 91 steel—a review of current code and fabrication practices*, Proceedings of the Sixth International Conference on Advances in Materials Technology for Fossil Power Plants, La Fonda, USA.

3. Wang, Y., Kannan, R., Li, L., (2016). *Characterization of as welded microstructure of heat affected zone in modified 9Cr–1Mo–V–Nb steel weldment*, Materials Characterization, 118, 225-234.

4. Wang, Y., Li, L., (2016). *Microstructure evolution of fine-grained heat affected zone in Type IV failure of P91 welds*, Weld. J., 95, 27-35.

5. Baral, J., Swaminathan, J., Chakrabarti, D., Ghosh, R.N., (2015). *Creep behavior of P91B steel in the presence of a weld joint*, Mater. Sci. Eng. A., 631, 220-229.

6. Łomozik, M., Tasak, E., (2006). *Physical simulation and numerical modelling of X10CrMoVNb 9.10 (P91) steel repair welding*, Proceedings of 8th Liege Conference on: Materials for Advanced Power Engineering, Liege, Belgium.

7. Porter, D.A., Easterling, K.E., Sherif, M., (2009). *Phase Transformations in Metals and Alloys*, CRC press, New York.

8. Wang, X.L., Tsai, Y.T., Yang, J.R., Wang, Z.Q., Li, X.C., Shang, C.J., Misra, R.D., (2017). *Effect of interpass temperature on the microstructure and mechanical properties of multi-pass weld metal in a 550-MPa-grade offshore engineering steel*, Weld. World, 61(6), 1155-1168.

9. Ciofu, C., Creţu, G., (2014). *Some aspects concerning the microindendation testing of ultramid plastic materials*, Int. J. of Mod. Manufact. Technol., VI(2), 11-14.

10. Yang, F., Li, J.C., (2013). *Impression test - A review*, Mater. Sci. Eng.: R., 74(8), 233 - 253.

11. Vijayanand, N.V., Ganesan, V., Laha, K., Mathew, M.D., (2014). *Evaluation of creep deformation behaviour of different microstuctural zones of 316LN SS weld joint using impression creep testing technique*, Mater. Sci. Technol., 30(10), 1223-1228.

12. Akhtar, M., (2017). *Metallurgical characterisation of simulated heat affected zone in boron modified P91 steel*, Master's dissertation, NIT Warangal, India.

13. Yu, H.Y., Li, J.C., (1977). *Computer simulation of impression creep by the finite element method*, Journal of Materials Science, 12(11), 2214-2222.

Received: November 3, 2017 / Accepted: June 15, 2018 / Paper available online: June 20, 2018 © International Journal of Modern Manufacturing Technologies.